Nanoscale

Effect of Chemical Substitution and External Strain on Phase Stability and Ferroelectricity in Two Dimensional M_2CT_2 MXenes

Journal:	*Nanoscale*
Manuscript ID	NR-ART-01-2022-000514.R1
Article Type:	Paper
Date Submitted by the Author:	12-Apr-2022
Complete List of Authors:	Li, Mo; New Jersey Institute of Technology, Chemical and Materials Engineering Omisakin, Olamide; New Jersey Institute of Technology, Chemical and Materials Engineering Young, Joshua; New Jersey Institute of Technology, Chemical and Materials Engineering

Journal Name

ARTICLE TYPE

Cite this: DOI: 00.0000/xxxxxxxxxx

Effect of Chemical Substitution and External Strain on Phase Stability and Ferroelectricity in Two Dimensional M_2CT_2 MXenes†

Mo Li,*[a] Olamide Omisakin,[a] and Joshua Young[a‡]

Received Date
Accepted Date

DOI: 00.0000/xxxxxxxxxx

Two dimensional ferroelectric materials are gaining increasing attention for use in ultrathin electronic devices owing to the presence of a spontaneous polarization down to one or two monolayers. However, such materials are difficult to identify, especially those with out-of-plane electric polarizations. Previous work predicted that a metastable ferroelectric phase exists in the 2D MXene Sc_2CO_2, while further studies have predicted that this phase exists in other MXene chemistries. However, questions remain about the origin of ferroelectricity, the stability of this phase relative to other competing phases, and the effect of external stimuli in these materials. In this work, we use density functional theory calculations to investigate 12 M_2CT_2 MXenes (M = transition metal, T = surface terminating group) and determine which have the ferroelectric phase as their ground state. We compute these materials' polarizations, densities of states, phonon band structures, Bader charges, and Born effective charges in the ferroelectric phase to elucidate the reasons for its stabilization. We demonstrate that this ferroelectric phase can be preferentially stabilized in non-ferroelectric MXenes through full chemical substitution of Sc or O, alloying of the Sc sites, or application of epitaxial strain. Finally, we show that these materials have excellent piezoelectric properties as well. This work provides a detailed understanding of ferroelectric MXenes and show how the number of 2D ferroelectric materials can be increased through chemical substitution or application of external stimuli.

1 Introduction

Ferroelectric materials have been actively studied for decades due to their controllable and switchable electronic characteristics. These materials display a spontaneous polarization that is reversible by applying an external electric field and have been utilized in a variety of significant applications, most notably nonvolatile memory[1–3] and field-effect transistors,[4,5] but also for hydrogen cells,[6] catalysis,[7–9] and energy storage[10,11]. Recently, however, the desire for increasingly smaller electronic components has driven a search for ultrathin ferroelectric materials. Typical bulk oxide ferroelectrics, such as $BaTiO_3$ or $PbTiO_3$, were long thought to be impossible to scale down, as they often lose their spontaneous polarization below a critical number of unit cells owing to suppression by a depolarizing field.[12] Although it was recently demonstrated that $BiFeO_3$ and PZT ($PbZr_{0.2}Ti_{0.8}O_3$) both retain a a spontaneous polarization even when approaching the 2D limit,[13,14] an alternative path to identify ultrathin ferroelectric is to look towards layered or van der Waals stacked materials as they are easier to exfoliate down to the monolayer.

Such so-called two-dimensional ferroelectric materials (2DFEs, or one-/few-layer materials which display a switchable electric polarization), have attracted increasing interest as ways to surpass Moore's Law. A wide variety of 2D materials have been discovered or predicted to be ferroelectric in the past years, such as transition metal dichalcogenides (*e.g.*, MoS_2 and $MoTe_2$),[15–19] hexagonal boron nitride (h-BN),[20] and In_2Se_3.[21–23] However, one significant challenge is finding 2DFEs such as CIPS ($CuInP_2S_6$)[24] or the aforementioned In_2Se_3 with large out-of-plane polarizations (which is better for device operation), as most discovered thus far display in-plane ones.

To this end, it was recently predicted by Chandrasekaran *et al.* from first principles calculations that the MXene compound Sc_2CO_2 displays a metastable ferroelectric phase with an out-of-plane polarization.[25] MXenes are a large family of materials that was first discovered from exfoliation of the conventional MAX phases by Naguib *et al.*,[26] and are typically carbides and nitrides with chemical formula $M_{n+1}X_n$, where M is a transition metal, X is carbon or nitrogen.[27–30] The unique structure and chemistry of MXenes has made them good candidates for a variety of applications such as water splitting,[31,32] Li-ion batteries,[33,34] and super-

[a] *Department of Chemical and Materials Engineering, New Jersey Institute of Technology, Newark, New Jersey 07102 USA*

† Electronic Supplementary Information (ESI) available: [details of any supplementary information available should be included here]. See DOI: 00.0000/00000000.

‡ Corresponding author. Email: jyoung@njit.edu

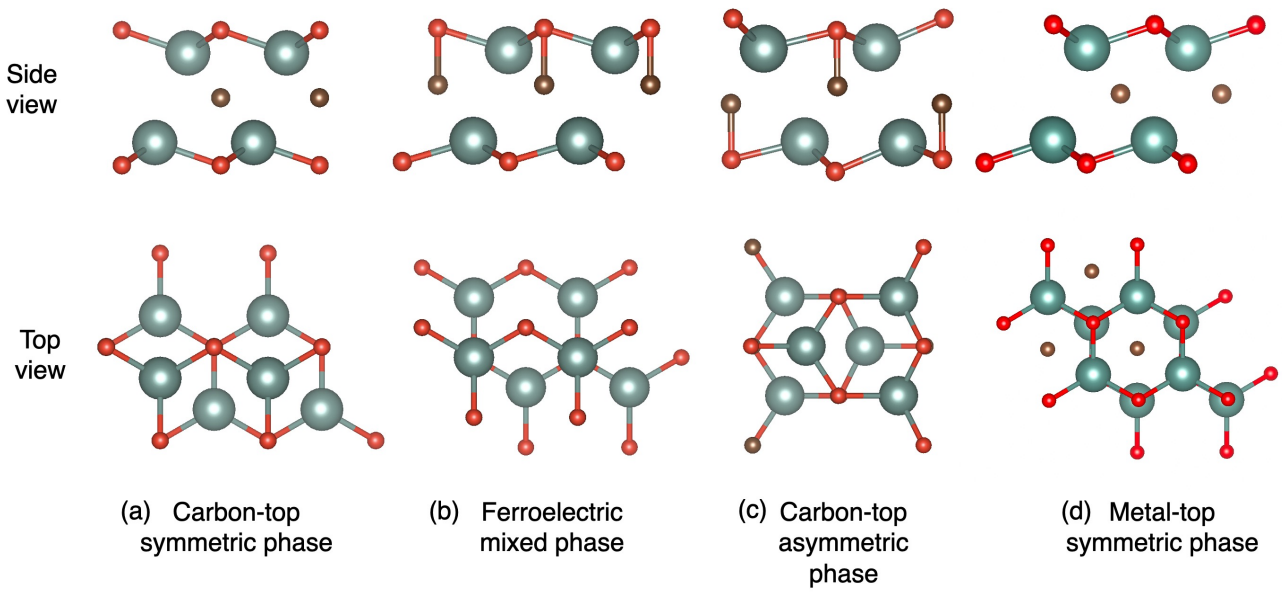

Fig. 1 Crystal structures for M_2XT_2 in the (a) carbon-top symmetric phase, (b) ferroelectric mixed phase, (c) carbon-top asymmetric phase, and (d) metal-top symmetric phase from the side and top. M atoms are green, X atoms are brown, and T atoms are red.

capacitors.[35] Furthermore, MXene surfaces can be functionalized to create $M_{n+1}X_nT_{n+1}$ compounds, where T is a surface termination group such as -O, -F, or -OH (although there are many other possibilities).[36] In the $n = 1$ case (such as the aforementioned Sc_2CO_2), the monolayer MXenes consist of five atomic layers: two layers of M interspersed with a layer of C or N, with a layer of T on both surfaces (Figure 1).[26,37–39] The relative orientation of the two T layers to one another and to the M/X atoms in the MXene influences the symmetry and structure, and therefore the properties, of the material.

Chandrasekaran *et al.* studied four possible phases with different T termination orientations, denoted as symmetric carbon-top, mixed, asymmetric carbon-top, and metal top (Figure 1a-1d, respectively); the naming convention comes from whether the T atoms are above or below the M or X atoms. While the symmetric carbon-top and metal-top phases form in a non-polar $P\bar{3}m1$ space group, the asymmetric carbon-top and mixed structures both display the polar $P3m1$ space group, allowing for the presence of a spontaneous electric polarization. Indeed, they found the mixed phase does display a small ferroelectric polarization (1 $\mu C/cm^2$), while the polarization in the asymmetric carbon-top phase is 0 owing to the alternating up and down displacements of the C atoms. However, the asymmetric carbon-top configuration is the ground state of Sc_2CO_2, making the ferroelectric mixed phase only metastable. Despite this, ferroelectric Sc_2CO_2 has been investigated for use in a number of applications such as gas sensors[40,41] and magnetoelectric devices and spintronics.[42,43]

Two further studies expanded upon these results. First, Zhang *et al.* performed a screening of 110 $M_{n+1}X_nT_{n+1}$ MXene chemistries, with M = Sc, Ti, V, Cr, Y, Zr Nb, Mo, Hf, Ta, W; X = C, N; and T = OH, S, O, F, Cl.[44] They computed the relative stability of each compound in the aforementioned metal-top, symmetric carbon-top, and mixed structure types, and found 9 cases where the ferroelectric mixed phase is lowest in energy: Sc_2CO_2, Y_2CO_2, Sc_2CS_2, Y_2CS_2, Nb_2CS_2, Ta_2CS_2, $Zr_2C(OH)_2$, $Hf_2C(OH)_2$, and Mo_2NCl_2. They then classify the resulting polar mixed phases into three types based on how the inversion symmetry is broken. This work showed it is possible to expand the number of possible 2D ferroelectric MXenes *via* chemical substitution. However, because the asymmetric carbon-top configuration was not considered in their work, some results are in contrast to the previous work by Chandrasekaran *et al.*, which predicts zero polarization in the Sc_2CO_2 ground state. Furthermore, Berry phase calculations were not used to compute the out-of-plane spontaneous polarizations.

Another study was performed by Wijethunge *et al.* in which they performed screening of 72 MXene structures to look for possible ferroelectric metals.[45] Interestingly, they found that Nb_2NF_2 has both a spontaneous polarization and metallic character, leading to a new potential 2D ferroelectric metal. However, although they investigated 6 different MXene surface termination and structure types, the asymmetric carbon-top configuration was again not considered as a possible polymorph; as such their study again found Sc_2CO_2 to have a ferroelectric ground state. Furthermore, no polarization magnitudes were reported.

Finally, a recent computational study was performed on Hf_2CF_2 by Wang *et al.*[46] Although this compound's ground state is the metal top configuration, the authors found that moderate compressive strain causes one layer of F to shift such that the compound is now in the mixed ferroelectric phase. This also causes the compound to go from metallic to semiconducting. They also found that the domain walls are metallic, and elucidated some possible polarization switching paths.

Although all of these works generate excellent insight into the

possible ferroelectricity in MXenes, a number of questions still remain, which we seek to answer in the work. Through the use of density functional theory (DFT), we systematically study a number of M_2CT_2 MXene carbides. For the transition metals, we selected Sc, Y, La, Ti, Zr and Hf; for the purpose of studying the effect of surface termination groups, we selected O, S, F, and Cl. Therefore, in this paper, we report detailed results for 12 MXene compositions as following: Sc_2CO_2, Sc_2CF_2, Sc_2CCl_2, S_2CS_2, Y_2CO_2, Y_2CF_2, Y_2CCl_2, Y_2CS_2, Zr_2CO_2, Hf_2CO_2, Ti_2CO_2, and La_2CO_2. For each of these, we first compute the relative energetic stability of each in the symmetric carbon-top, mixed, asymmetric carbon-top, and metal-top configurations shown in Figure 1, finding that 3 have the ferroelectric mixed phase as their ground state. However, to better understand the origin of ferroelectricity in this family of materials, we perform a detailed analysis of all compounds in the ferroelectric phase by computing their polarization, density of states, Bader charges, dielectric and piezoelectric properties, and Born effective charges. We find that polarization arising from C off-centering is caused by a hybridization of the C and O atoms, and that Sc/Y and O/S is required for stabilization of a ferroelectric phase. Finally, we investigate the effect of alloying on the M site and application of external strain in Sc_2CO_2, and show that both can be used to preferentially stabilize the ferroelectric phase. These results demonstrate numerous new possible routes to the stabilization of the ferroelectric mixed phase in surface functionalized MXenes.

2 Computational Details

The first principles density functional theory (DFT)[47] calculations were performed by the Vienna *ab initio* Simulation Package (VASP) using the projector augmented wave (PAW) methods[48].[49] The general gradient approximation introduced by Perdew, Burke and Ernzerhof (PBE-GGA) was adopted to describe the exchange correlation.[50] A 550 eV plane wave cutoff was used for all calculations. Geometry optimizations were performed for each chemistry in four different phases (symmetric carbon-top, mixed, asymmetric carbon-top, and metal-top, Figure 1). Due to the shape difference of the unit cell, the Monkhorst-Pack k-point mesh of $15\times30\times1$ was used for the asymmetric carbon-top phase, while $30\times30\times1$ was used for the symmetric carbon-top, mixed, and metal-top phases. In order to avoid the interaction between vertically repeated unit cells, more than 15 Å of vacuum was included for each structure. Considering the fact that the PBE approximation typically underestimates the band gaps, the Heyd–Scuseria–Ernzerhof (HSE06) hybrid functional was adopted for calculating the band gaps.[51,52] A less dense k-point grid of $4\times4\times1$ was used for all HSE calculations. The dynamical stability of our fully relaxed geometries were checked using density functional perturbation theory (DFPT) and the Phonopy code.[53] DFPT was also used to compute the piezoelectric constants and Born effective charges. The spontaneous polarization was calculated by the Berry phase method.[54] The Bader charge calculations were performed using the code from Henkelman *et al.*[55–57] The piezoelectric strain was calculated based on the stress tensor and the compliance tensor (inverse of the elastic tensor). The expression of the calculation is: $d_{ij} = e_{ik} \times S_{kj}$.

3 Results and Discussion

3.1 Structures and Phases of MXenes.

We first investigated the structures of 12 2D single layered M_2CT_2 compounds: Sc_2CO_2, Sc_2CF_2, Sc_2CS_2, Sc_2CCl_2, Y_2CO_2, Y_2CF_2, Y_2CS_2, Y_2CCl_2, Zr_2CO_2, Hf_2CO_2, Ti_2CO_2, and La_2CO_2. These were chosen because both O- and S-termination often lead to the ferroelectric phase while F- and Cl- often does not,[44] and our goal is to investigate the reasons for this competition. We did not select the -OH group for investigation here because, although such termination can result in the mixed phase being stable, this only happens for the Zr and Hf compounds which does not lead to the necessary C displacements for a large spontaneous ferroelectric polarization.[44] Finally, we note that recent work has opened up the potential for such exotic terminations on MXenes; for example, Kamysbayev *et al.* used novel exchange reactions to experimentally synthesize Ti_2C and Ti_3C_2 MXenes terminated with O, S, Se, Te, F, Cl, and NH groups.[58]

Previous studies reported four major phases for 2D single layered MXene materials (Figure 1),[25,59,60] which are the carbon-top symmetric phase (symmetric), ferroelectric mixed phase (mixed), metal-top asymmetric phase (asymmetric), and metal-top symmetric phase (M-top). The structural differences among the four phases arise from the relative position of their surface termination layers. As can be seen from the top view of Figure 1, O atoms in both the top and bottom layer are above the C atoms in the two carbon-top phases, while in the M-top phase the O atoms sit above M atoms in both layers. The mixed phase (Figure 1b) is unique in that one O layer is above the M atoms while one is above C atoms. Because of these differences in coordination, the symmetric phase and the M-top phase are centrosymmetric (space group $P\bar{3}m1$), whereas the mixed phase and the asymmetric phase are non-centrosymmetric (space group $P3m1$) and can exhibit ferroelectricity.[61] Indeed, in the mixed phase (Figure 1b), all C atoms can cooperatively shift, resulting in a spontaneous electric polarization. In the asymmetric phase, however, the alternating up and down C displacements cancel, leading to a net zero polarization.

	asymm.	mixed	symm.	M-top
Sc_2CO_2	0	8.997	32.58	155.8
Sc_2CS_2	117.9	0	359.4	1211
Sc_2CF_2	221.5	95.66	220.3	0
Sc_2CCl_2	155.4	75.39	155.4	0
Y_2CO_2	1.501	0	26.39	90.59
Y_2CS_2	200.9	0	440.9	1258
Y_2CF_2	202.0	97.72	202.0	0
Y_2CCl_2	120.0	58.07	120.1	0
Zr_2CO_2	526.6	384.3	171.3	0
Hf_2CO_2	660.2	192.5	428.4	0
Ti_2CO_2	315.2	99.01	291.5	0
La_2CO_2	104.7	0	22.44	98.27

Table 1 Relative total energies (meV/atom) for each MXene composition in each of the four phases with respect to their lowest energy phase.

We calculated the total energies per atom for the 12 studied materials under the four different phases using DFT by fully opti-

mizing the lattice parameters and atomic positions of each (Table 1). The relaxed geometries of the Y_2CO_2 MXene are shown in Figure 1a-d, while those of all materials are given in the Supplemental Information as Figures S1-S9. For most of the compositions, the M-top phase is the energetically favorable phase, in agreement with the aforementioned previous works.[44,45] The asymmetric phase is the most energetically favorable phase for Sc_2CO_2, which shows agreement with the original work by Chandrasekaran *et al.*[25] In contrast, Y_2CO_2 is more stable in the mixed configuration, although the asymmetric phase is higher in energy by a very small 1.5 eV/atom. The three other compounds which display a non-M-top phase as their ground state are Sc_2CS_2, Y_2CS_2 and La_2CO_2.

Because we are interested in the possibility of a stable or metastable ferroelectric phase, we computed the phonon band structures for each compound in the mixed phase (Supplemental Figures S18-S28). All materials except three display no negative frequencies (the observed very small negative frequencies near the Γ-point are likely caused by numerical noise owing to the vacuum region[62]). The three exceptions (Sc_2CS_2, Y_2CS_2 and La_2CO_2) all display significant negative frequencies in their phonon band structure (Supplemental Figures S20, S23, and S24, respectively), as previously discussed by Zhang *et al.* (at least for Sc_2CS_2 and Y_2CS_2). Following their procedure, we froze the atomic displacements corresponding to these negative modes into the three structures, and re-optimized them; in agreement, Sc_2CS_2 and Y_2CS_2 actually show some antisymmetric displacements of the Sc/Y and S atoms (Figure 2a and b, respectively), although the cooperative displacements of the C atoms are still present. The energies of these phases are the ones reported in Table 1, and this structure was used for all subsequent calculations involving Sc_2CS_2 and Y_2CS_2. This procedure did not work for La_2CO_2, implying its mixed phase is dynamically unstable. Finally, none of the materials showed the symmetric phase as the ground state. Our results of the predicted ground states now result in complete consistency between the works on ferroelectricity in MXenes by Chandrasekaran *et al.*, Zhang *et al.*, and Wijethunge *et al.*[25,44,45]

Interestingly, for every compound that displays the M-top configuration as its ground state, the mixed phase is the next lowest in energy (with the exception of Zr_2CO_2). This energy difference between the M-top and mixed phases is the smallest in the M = Sc and Y compounds with monovalent anions (F, Cl). Ti_2CO_2 has a slightly larger difference than these, with Hf_2CO_2 having the largest of the studied compounds. As such, as reported for Hf_2CF_2 by Wang *et al.*,[46] it should be relatively easy to stabilize the mixed phase with external stress.

We put our results in the context of the potential for stabilization of these ferroelectric phases in the functionalized M = Sc and Y MXene carbides; to the best of our knowledge such systems have not been experimentally realized but have been studied computationally for a variety of applications.[40,41,43,63–65] Although the phonon band structures indicate dynamic stability of this phase in these compounds, the ability to chemically synthesize these materials should be discussed as oxycarbides can be difficult to create. Several studies have investigated the thermodynamic stability of some of these MXenes, which we review here; we note, however, that these studies did not study or propose the ferroelectric phase.

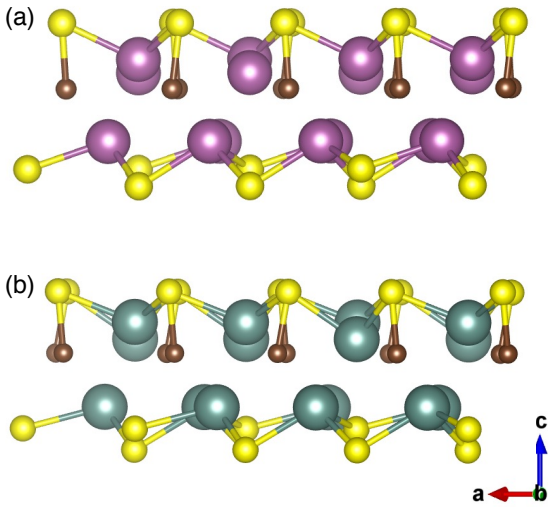

Fig. 2 Structure of the mixed (a) Sc_2CS_2 and (b) Y_2CS_2 phases.

First, Khazaei *et al.* used DFT calculations to predict the stability of various M_2X carbides and nitrides functionalized by T = O, F, and OH groups. By computing the formation energy (ΔH) of a functionalized MXene with respect to the unfunctionalized monolayer and T_2 gas molecule, they found that Sc_2C functionalized with any of these is stable with a negative ΔH (the stability order is Sc_2CF_2 > $Sc_2C(OH)_2$ > Sc_2CO_2).[66] A later study by Xiong *et al.* also investigated Sc_2CT_2 with these same T species and found that the cohesive energy for each (*i.e.*, the energy of Sc_2CT_2 relative to the constituent Sc, C, and T atoms by themselves) is similar to many other 2D materials, further indicating the possibility for the stability of these compounds.[67] However, a study Ashton *et al.* found that, although the binding energy for T atoms to Sc_2C surfaces are negative (*i.e.*, favorable), and that functionalization by F over O is preferred, computing ΔH with respect to the most stable compound with the same stoichiometry gave a very large (*i.e.*, unfavorable) value of 0.7 eV/atom for Sc_2CO_2.[68] Therefore, a ferroelectric Sc_2CT_2 has the potential to be stable relative to the constituent parts, but questions remain about whether this monolayer would thermodynamically form in this phase. Furthermore, these results indicate that Sc_2CF_2 should be easier to synthesize than Sc_2CO_2, but the ferroelectric phase is not the ground state. However, the ferroelectric phase in Sc_2CF_2 is 100 meV/atom lower in energy than the ground state, so a similar approach of applying external stimuli as in Hf_2CF_2[46] could potentially be used.

Functionalization of Sc_2C by S has been significantly less studied,[69] although it should be possible given the large amounts of species shown to be possible to functionalize Ti_2C and Nb_2C.[70] Finally, while the Y_2C monolayer has been predicted to be stable by DFT calculations,[71] any functionalization of it has not been investigated except for the aforementioned ferroelectric MXene studies. It is therefore difficult to anticipate stability of these compounds, but we anticipate that similar results would hold for the

	E_g (eV)		P (μC/cm^2)	Bader Charge							b_{C-T1} (Å)
	PBE	HSE		**C**	**M1**	**M2**	**T1**	**T2**	**ΔM**	**ΔT**	
Sc_2CO_2	1.81	2.73	0.64	-1.07	1.55	1.69	-1.02	-1.15	0.14	0.13	2.19
Sc_2CS_2	1.50	1.91	0.52	-1.40	1.40	1.53	-0.58	-1.40	0.13	0.82	1.94
Sc_2CF_2	0.95	1.47	0.17	-1.75	1.58	1.61	-1.72	-1.72	0.03	0	2.27
Sc_2CCl_2	0.74	1.43	0.08	-1.81	1.52	1.54	-0.62	-0.62	0.02	0	2.33
Y_2CO_2	1.35	2.07	0.58	-1.32	1.88	2.00	-1.17	-1.38	0.12	0.21	2.38
Y_2CS_2	1.50	2.19	0.49	-1.54	1.74	1.83	-0.77	-1.23	0.09	0.46	2.49
Y_2CF_2	1.05	1.53	0.21	-2.12	1.86	1.92	-1.82	-1.82	0.06	0	2.53
Y_2CCl_2	0.96	1.38	0.06	-2.15	1.79	1.82	-0.72	-0.73	0.03	0.01	1.97
Ti_2CO_2	0.67	1.31	0.05	-1.46	1.65	1.73	-0.95	-0.96	0.08	0.01	2.19
Hf_2CO_2	1.07	1.65	0.04	-1.80	1.98	2.07	-1.11	-1.13	0.09	0.02	2.21

Table 2 The band gaps (E_g, eV) for MXene compositions in the mixed phase using PBE and HSE06 methods. Magnitude of the out-of-plane spontaneous electric polarization (P, μC/cm^2) in the mixed phase of each compound. Bader charges for each element in the MXene compositions in the mixed phase, where **C** represents the carbon atom, **M1** and **M2** represent the transition metal (Sc, Y Hf and Ti) in the top layer and bottom layer, respectively, and **T1** and **T2** represent the surface termination group (O, S, F and Cl) at the top layer and bottom layer, respectively.

Y-based compounds as the Sc-based ones owing to their relative positions in the periodic table. Finally, despite concerns about stability of these materials, it is instructive to investigate the ferroelectricity, piezoelectricity, and electronic structure in these compounds fully to understand their properties and the origin of the potential ferroelectricity.

3.2 Polarization and Ferroelectricity

We first computed the polarization (P) for each MXene composition that has a stable mixed ferroelectric phase as their ground state or second lowest energy phase (Table 2). We obtained out-of-plane spontaneous polarizations and found the largest polarization in the Sc_2CO_2 mixed phase (0.64 $\mu C/cm^2$). This is smaller than that reported by Chandrasekaran *et al.*[25] (1 $\mu C/cm^2$), but relatively close; computation of the polarization quantum shows this value is accurate in our case (Supplemental Figure 30). Upon substitution of the anion, we find that the polarization decreases, with the trend that $Sc_2CO_2 > Sc_2CS_2 > Sc_2CF_2 > Sc_2CCl_2$. Therefore, substitution of O by a larger species (S) causes the polarization to decrease. Substitution of Sc by a larger atom (Y) causes a small decrease in the polarization, but not nearly as pronounced as anion substitution. Indeed, the second largest polarization is observed in Y_2CO_2 (0.58 $\mu C/cm^2$), and a similar trend appears for anion substitution in these Y-based MXenes. Finally, in La_2CO_2, the C displacements are still present; however, we did not compute the polarization owing to the fact that the ferroelectric phase is dynamically unstable.

As mentioned above, substitution of a divalent T species with a monovalent one (F or Cl) results in a loss of the off-centering C displacements. This also occurs in the case of substitution of Sc/Y by Ti or Hf, which results in a polarization of almost zero. As can be seen by the structure in the aforementioned Supplemental Information, this is because upon optimization of the mixed phase of Sc_2CF_2, Y_2CF_2, Sc_2CCl_2, Y_2CCl_2, Hf_2CO_2, and Ti_2CO_2, the C atoms no longer cooperatively displace. Interestingly, in both M = Sc and Y, while replacement by Cl results in a near complete loss of P as expected, the F-based compounds still display a non-negligible polarization despite the fact that the off-centering C displacements are not present.

In addition to the magnitude of the polarization, questions still remain about its appearance in these MXene materials, as detailed analyses of the ferroelectric phase transition have not been performed. Here, we discuss Y_2CO_2 as a representative example as it has the ferroelectric mixed phase as its ground state. We first computed the phonon band structure of the symmetric Y_2CO_2 phase (Supplemental Figure S31), which, like Sc_2CO_2, shows negative frequencies at the M and K point.[72] An analysis of these unstable modes show that they both have off-centering of the C atoms, with the K mode actually leading to a polar $P3m1$ space group. This shows that, in the symmetric phase: (1) the C off-centerings are energy lowering displacements leading to the ferroelectric phase, and (2) these cooperative C displacements alone are sufficient to break inversion symmetry. However, these C displacements driving the phase transition must be coupled with some shifting of the O displacements to lead to the observed mixed phase; indeed, this cooperative motion was investigated by Chandrasekaran *et al.*[25] during the Sc_2CO_2 ferroelectric switching pathway calculations and can be observed in the video provided in their Supplemental Information. Using the ISODISTORT software,[73] we further investigated the $P\bar{3}m1$ symmetric Y_2CO_2 phase and found that there are M^{2-} and K_3 modes which have cooperative C displacements and lead to a $P3m1$ space group. There is also a possible Γ^{2-} mode consisting of such displacements and leading to a $P3m1$ space group, but there are no unstable frequencies at the Γ-point in the symmetric phase of these materials. While this analysis gives some insight into the appearance of the spontaneous polarization in these materials, a more detailed analysis of the phase transition mechanism should be performed to fully understand these materials.

Finally, it is worthwhile to discuss the details of the ferroelectric switching mechanisms in these materials. Because this has been extensively studied in previous works,[25] we will not repeat the calculations here but provide a summary and put them in context of our new results here. In general, these materials switch by a cooperative switching of the C displacement direction and a lateral shift of the bottom X-termination layer. However, the details are more complex. First, Chandrasekaran *et al.*,[25] using nudged elastic band (NEB) calculations, showed that Sc_2CO_2 switching

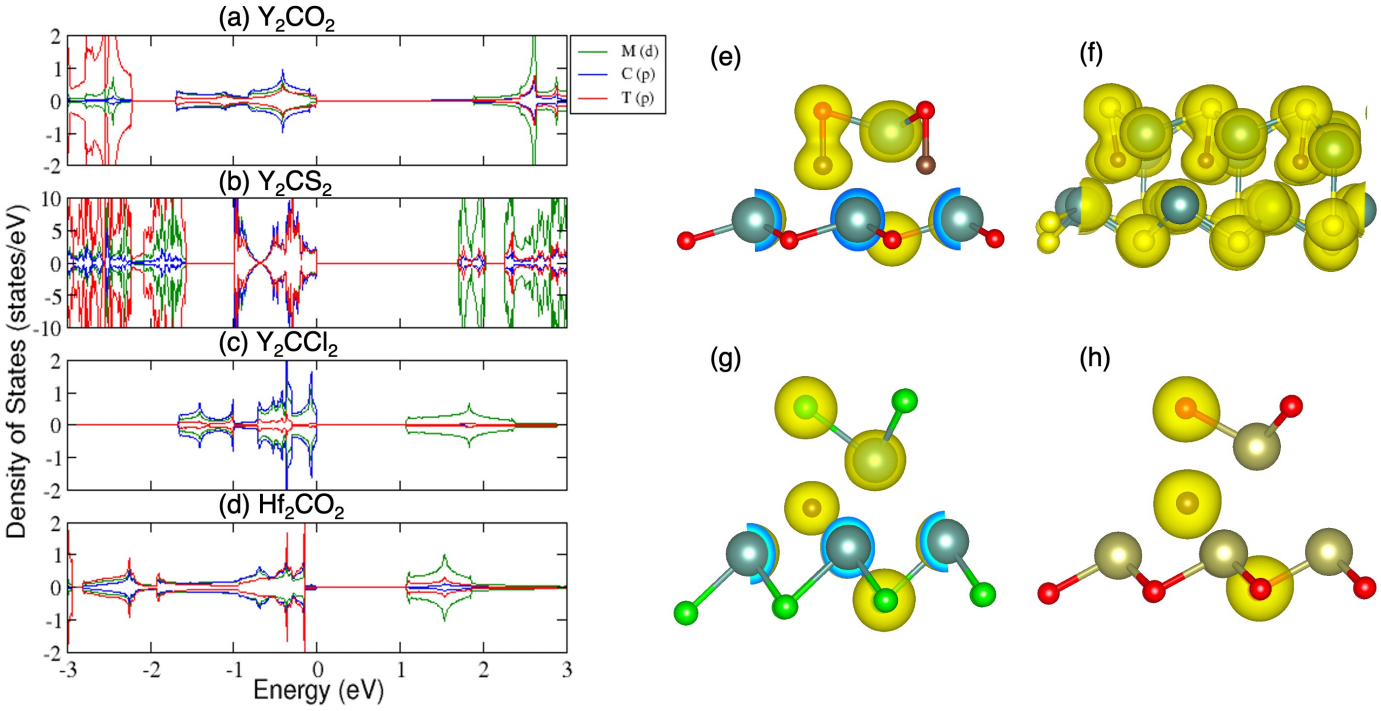

Fig. 3 Decomposed density of states for (a) Y_2CO_2, (b) Y_2CS_2, (c) Y_2CCl_2 and (d) Hf_2CO_2. Spin up and spin down density of states are both shown. Charge density contours for (e) Y_2CO_2, (f) Y_2CS_2, (g) Y_2CCl_2 and (h) Hf_2CO_2. Region in yellow represents the negative charge cloud.

proceeds *via* a two-step mechanism. The poled-up ferroelectric phase first transitions to a carbon-top anti-ferroelectric phase over a 0.52 eV barrier through a symmetric phase; overcoming a second 0.52 eV barrier transforms this into the poled-down ferroelectric phase. Zhang *et al.*[44] followed up on this and also used NEB calculations to study the switching of a number of other MXene ferroelectrics. First, they found that Y_2CO_2 goes through the same two-step switching procedure through an anti-ferroelectric phase as Sc_2CO_2 with a similar barrier (0.53 eV). Sc_2CS_2 and Y_2CS_2 (also investigated in this work) also proceed the same way with barriers of 0.53 eV and 0.57 eV, respectively, although the anti-ferroelectric intermediate is much higher in energy than either of the ferroelectric end points; this is in agreement with our energy calculations showing that the difference in energy between the asymmetric and mixed phases in Sc_2CS_2 and Y_2CS_2 is two orders of magnitude higher than in the equivalent X = O compounds. Overall, the compounds which the ferroelectric mixed phase as their ground state show relatively small switching barriers of approximately 0.5 eV.

3.3 Electronic Structure

We next computed the density of states (DOS) of each compound in each phases. First, both PBE and HSE06 were used to calculate the band gaps; the values for all of the mixed phases are shown in Table 2. The total DOS at the PBE level for all compounds in each phase are shown the Supplemental Information as Figures S10-S17. As expected, the PBE band gaps are much lower than the HSE band gaps, in agreement with the fact that typical DFT methods underestimate them. Due to the correction from the Hartree-Fock method, values from the HSE06 method are closer to the experimental values and become a more reliable result in understanding the band gaps of our materials. According to Table 2, the values from the HSE calculations range from 1.3 eV to 2.7 eV, showing that these MXene compositions all have semiconducting band gaps in their mixed phase. Replacing Sc with Y does not have a significant effect on the band gap; in both the Sc- and Y- based compounds, however, substitution of the divalent anions (O, S) with monovalent ones (F, Cl) results in a significant band gap reduction.

Next, as shown in Figure 3a-d, orbital-decomposed DOS were plotted for Y_2CO_2, Y_2CS_2, Y_2CCl_2, and Hf_2CO_2. As predicted by Chandrasekaran *et al.*[25], the polarization in the mixed phase is likely induced by C-O hybridization. This is observed in the DOS of Y_2CO_2 (Figure 3a) and Y_2CS_2 (Figure 3b), where both C(p) and O(p)/S(p) orbitals overlap near the Fermi level to around -1 or -2 eV. On the other hand, no overlap between C and Cl are observed in the Y_2CCl_2 DOS (Figure 3c). A similar effect is observed in Hf_2CO_2, with little C-O orbital overlap resulting in no displacement of the C atoms. This can also be seen in a plot of the charge density for the compounds, where large amounts of charge can be seen along the C-O and C-S bond in Y_2CO_2 and Y_2CS_2 (Figure 3e and 3f, respectively). As can be seen in Figure 3g and 3h, the charge density remains centered on each atom in Y_2CCl_2 and Hf_2CO_2, and the C atoms do not displace in thse compounds.

Finally, we computed the average Bader charges of each element in the mixed phase compositions, which are reported in

	Piezoelectric coefficients			Born effective charges				Dielectric constants			
	Index	e (C/m^2)	d (pC/N)	Atom	Z^*_{11}	Z^*_{22}	Z^*_{33}	Index	ε^{elec}	ε^{ion}	ε^{tot}
Sc_2CO_2	15	0.06	244	C	-2.84	-2.84	-0.11	11	3.49	2.33	5.81
	22	0.26	10.3	O1	-1.43	-1.44	-0.61	22	3.49	2.33	5.81
	31	0.03	0.33	O2	-3.07	-3.07	-0.52	33	3.14	0.02	3.16
	33	0.01	16.5	Sc1	4.10	4.10	0.63				
				Sc1	3.25	3.25	0.61				
Y_2CO_2	15	0.05	193	C	-2.80	-2.77	-0.14	11	2.39	1.77	4.16
	22	0.32	13.3	O1	-1.52	-1.49	-0.70	22	2.39	1.76	4.15
	31	0.04	0.51	O2	-2.90	-2.90	-0.59	33	1.26	0.07	1.33
	33	-0.02	-6.90	Y1	3.90	3.91	0.73				
				Y2	3.32	3.26	0.70				
Sc_2CS_2	15	0.03	340	C	-2.81	-2.81	-0.17	11	3.49	2.33	5.81
	22	0.48	42.7	S1	-1.27	-1.27	-0.22	22	3.49	2.32	5.81
	31	0.02	0.35	S2	-2.79	-2.79	-0.28	33	3.14	0.02	3.16
	33	0.01	30.6	Sc1	4.16	4.16	0.31				
				Sc2	2.71	2.71	0.35				
Y_2CS_2	15	0.02	398	C	-2.78	-2.78	-0.23	11	2.77	1.95	4.72
	22	0.43	126	S1	-1.35	-1.35	-0.27	22	2.77	1.95	4.72
	31	0.02	0.38	S2	-2.69	-2.69	-0.35	33	2.54	0.02	2.56
	33	0.01	50.3	Y1	4.02	4.02	0.40				
				Y2	2.80	2.80	0.44				

Table 3 The computed results of piezoelectric coefficients at selected matrix index. The Born effective charges Z^* at the diagonal positions of the matrix and the dielectric constants are also presented.

Table 2. **T1** and **T2** represent anions (O, S, F and Cl) in the top layer and bottom layer, while **M1** and **M2** represent the same for the metal atoms (Sc, Y, Hf, and Ti); $\Delta\mathbf{M}$ and $\Delta\mathbf{T}$ represent the absolute difference in the Bader charge between the M and T layers, respectively. In general, it is expected that the charge on the top and bottom layers of terminating anions and metals should be the same without any distortions (*i.e.*, $\Delta\mathbf{M}$ and $\Delta\mathbf{T}$ are close to zero); indeed, this is what we find for the mixed phases of compounds with near zero polarization (Sc_2CCl_2, Y_2CCl_2, Ti_2CO_2, and Hf_2CCl_2). Interestingly, we also find that $\Delta\mathbf{T} = 0$ in the T = F phases as expected since they do not have any C displacements; as mentioned before, however, they do display a small non-zero polarization. Only in the compounds which do not have the M-top phase as their ground state (Sc_2CO_2, Sc_2CF_2, Y_2CO_2, and Y_2CS_2) is $\Delta\mathbf{T}$ non-zero; as expected, it is much larger in the T = S compounds which have anti-symmetric S displacements. However, in both the M = Sc and Y families $\Delta\mathbf{M}$ increases and **C** gets more negative as the polarization increases. Finally, we report the average C-T bond length in each compound (Table 2), although there is not a strong correlation with magnitude of the polarization.

3.4 Piezoelectric Tensors

As shown in the previous sections, we obtained the out-of-plane polarization in the mixed phase of MXene compositions, which was generated due to the cooperative off-centering of C atoms. However, all ferroelectric materials are also piezoelectric. Therefore, to further understand these materials' electronic properties, we calculated their piezoelectric stress (e_{ij}) and piezoelectric strain (d_{ij}) coefficients, as well as their dielectric constants (Table 3). There are eight components in the P3m1 (point group 3m) piezoelectric tensor, with four of them being independent. In this section, only compositions having mixed phase as the ground state will be discussed, which are Y_2CO_2, Sc_2CS_2 and Y_2CS_2. Sc_2CO_2 has mixed phase as a meta-stable phase, but since the energy difference between its ground state phase and meta-stable phase is relatively low, the piezoelectric properties are also important to study. Interestingly, all four of these compounds display a relatively large d_{33} component (ranging from 6.9 to 50 pC/N), which is best for device applications. The largest component in each case is the off-diagonal d_{15}, while the smallest is d_{31} Finally, all calculated piezoelectric tensor compounds are larger in the T = S compounds than the T = O compounds; this is likely related to the fact that these materials have slightly smaller polarization, meaning larger polarizations can be caused from external stress and strain.

We next computed the Born effective charges (BEC) for each compound (Table 3). In prototypical ferroelectrics such as $BaTiO_3$, the BECs are anomalously large (*i.e.*, above +7 for Ti^{4+} and nearly -5 for O^{2-}).[74] For all studied MXene compounds here, the out-of-plane BECs (Z^*_{33}) of all atoms are much smaller than their nominal value (less than -1 for C and T and less than +1 for M). This is in agreement with calculations on other 2D ferroelectrics like In_2Se_3, which also display much smaller than excepted out-of-plane BECs.[75,76] Indeed, this is similar to the family of hyperferroelectrics investigated by Garrity *et al.*;[77] in such materials, small out-of-plane BECs lead to a weak depolarization field and therefore can be polarized even when the depolarization field is unscreened. As such, small Z^*_{33} in 2D ferroelectrics such as the MXenes studied here is one reason for the presence of a spontaneous out-of-plane polarization even down to the monolayer.

The in-plane BEC (Z^*_{11} and Z^*_{22}), on the other hand, are not anomalously small; because Z^*_{11} and Z^*_{22} are nearly equivalent

in all studied materials here, we will not distinguish between them in this discussion. In the MXene compounds which have the mixed ferroelectric or asymmetric antiferroelectric phase as their ground state (those shown in Table 3), the average in-plane BECs of each atomic species do not deviate significantly from the excepted oxidation state of +3 for Sc/Y, -2 for C, and -2 for O/S. We do point out, however, the in-plane BECs depend on the layer of the atoms; the Sc/Y (O/S) atoms that are in the top layer (*i.e.*, closer to the displaced C atoms) are more positive (less negative) than those in the bottom layer. When we look at the average in-plane BECs of the mixed phase MXenes which do not show that phase as their ground state (Supplemental Information, Table S1), we find slightly different results. The expected oxidation states for the Sc- and Y-based monovalent anion compounds are +3 for Sc/Y, -4 for C, and -1 for F/Cl. Here, although the F/Cl atoms average in-plane BECs are -1.3 to -1.4, those for the Sc/Y atoms are above +4 (in addition, the layer dependence of the BECs is still present); for C in these compounds it is below -5. On the other hand, in Ti_2CO_2 and Hf_2CO_2, the average in-plane BECs are slightly higher than expected for M (5.47 for Ti^{4+} and 5.09 for Hf^{4+}) while for C it is around -4.4 in both (close to the nominal value of -4).

Finally, we computed the dielectric constants (ε^{tot}, Table 3) for each MXene in the mixed phase. In each material, ε^{tot} is small (less than 6). Furthermore, the out-of-plane dielectric constant is less than 50% of the in-plane dielectric constants. This is also similar to other 2D ferroelectrics like In_2Se_3, which, when scaled down to the monolayer display small dielectric constants.[76]

3.5 External Strain and Alloying

Finally, we investigated the possibility of preferentially stabilizing the mixed ferroelectric phase in Sc_2CO_2. First, we applied tensile and compressive biaxial strain to the two lowest energy phases of Sc_2CO_2 (mixed and asymmetric) from -2% to 2% in increments of 0.5%; at each point, the in-plane lattice parameters were fixed and the atomic position fully optimized. The total energy as a function of in-plane lattice parameter is shown in Figure 4a. Although the asymmetric phase remains the most stable under compressive strain, the ferroelectric mixed phase become more stable under only 0.5% tensile strain. Similar to the work by Wang *et al.*,[46] the application of external strain resulted in a shift of one layer of the terminating O atoms from being over the C atoms to being over the Sc atom; because the other layer remained over the C atoms, the mixed phase results. This is in contrast to the previously studied Hf_2CF_2 monolayer, which switched from the metal top to the mixed configuration, rather than C-top as shown here. This difference also likely partly contributes to the fact that compressive strain is needed for Hf_2CF_2, while tensile strain is needed for Sc_2CO_2.

We next investigated alloying Sc_2CO_2 and Y_2CO_2 together to create a series of mixed $Sr_{2(1-x)}Y_{2x}CO_2$ phases (x = 0, 0.25, 0.5, 0.75, and 1). In many 2D materials, alloying of both cations and anions has been shown to be a good way to preferentially stabilize metastable phases and tune their properties.[62,78–80] To determine the most energetically favorable Sr/Y position in each alloy

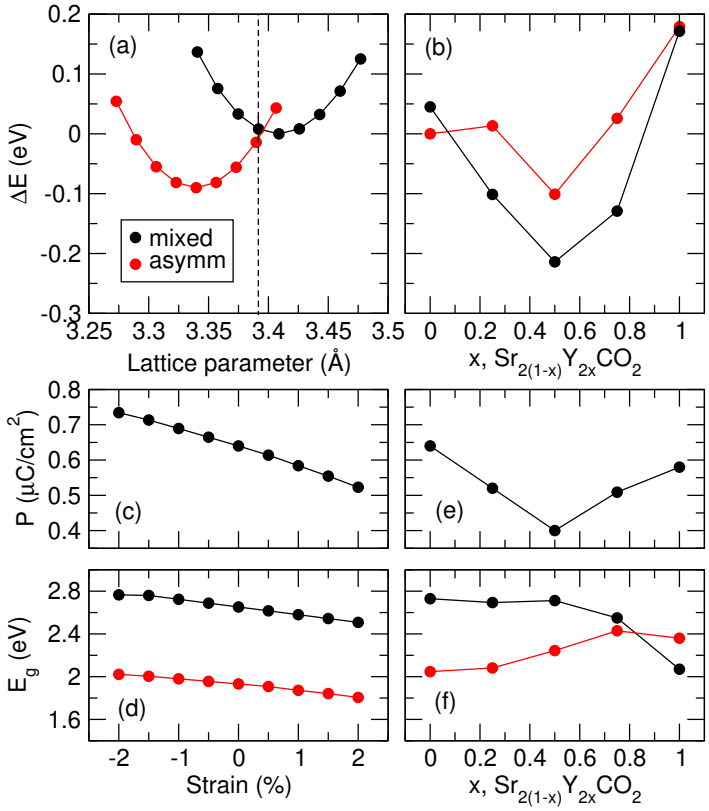

Fig. 4 (a) Relative energy (ΔE) of Sc_2CO_2 in the mixed (black) and asymmetric (red) phases as a function of lattice parameter. The dashed line indicates zero strain. (b) Relative energy of $Sr_{2(1-x)}Y_{2x}CO_2$ phases in the mixed and asymmetric phases as a function of concentration. (c) Change in polarization in Sc_2CO_2 as a function of strain. (d) Change in the band gap of the mixed and asymmetric phase of Sc_2CO_2 as a function of strain. (e) Change in the polarization of $Sr_{2(1-x)}Y_{2x}CO_2$ as a function of concentration. (f) Change in band gap of the mixed and asymmetric phase of $Sr_{2(1-x)}Y_{2x}CO_2$ as a function of concentration.

we tested all possible relative orientations and took the lowest energy one; all structures tested at each concentration in the mixed and asymmetric phases are shown in Supplemental Figures S28 and S29, respectively, with the lowest energy one highlighted. After fully relaxing each alloy in the mixed and asymmetric crystal structures, we found that although the asymmetric phase is the most favorable for Sc_2CO_2 (as previously discussed), the ferroelectric mixed phase becomes more stable at all concentrations of Y investigated. Because of this, the energy difference between the mixed and asymmetric phase is larger in the alloys than it is in Y_2CO_2; this indicates that this could be another route to the preferential stabilization of this phase since the two won't compete as strongly. Finally, calculation of the convex hull demonstrates that each of these alloyed phases is thermodynamically stable (Supplemental Figure S27).

Following this, we computed the change in the polarization and band gap (at the HSE level) upon application of strain. First, we found that compressive strain increases the polarization of Sc_2CO_2 (0.75 $\mu C/cm^2$ at -2% strain), while tensile strain decreases it (0.52 $\mu C/cm^2$ at 2% strain). This is shown in Figure 4c. As the lattice parameter shrinks, the magnitude of the C dis-

placements gets larger, and correspondingly get smaller as the lattice expands; this could also point to an explanation as to why the polarization of Sc_2CO_2 and Sc_2CS_2 are larger than Y_2CO_2 and Sc_2CS_2. However, because the mixed phase is only stable under tensile strain, any observed polarization is likely to be smaller than expected from DFT calculations. The band gap also changes monotonically as a function of strain (Figure 4d), with compressive strain resulting in a band gap opening and tensile strain resulting in a shrinking. Overall, however, the change in the band gap under strain is small, only 0.26 eV for the mixed phase and 0.22 for the asymmetric phase.

We then investigated these same property changes upon alloying of the Sc site with Y. Interestingly, the polarization decreases upon substitution or 25% Y and reaches a minimum at the equal 50% Sc/Y mixture (0.40 $\mu C/cm^2$), before increasing again as the Y concentration becomes larger (Figure 4e). An analysis of the structure shows that the magnitude of the C displacements do not change significantly, so this seems to solely be due to changes in the *M* atoms; indeed, as shown in Table 2, the charge density distribution (as found using Bader charge calculations) is different for the atoms in Sc_2CO_2 and Y_2CO_2, which can lead to the observed changes to the polarization. The band gap changes are slightly different in the alloying case than the strained case. In the mixed phase, the changes are quite small up to the 75% Y compound, at which point it begins to decrease as the band gap in mixed Y_2CO_2 is lower than Sc_2CO_2. However, in the asymmetric phase, the reverse is true as the band gap of Y_2CO_2 is higher than Sc_2CO_2; there is a dramatic increase of 0.4 eV from low to high Y concentration. Overall, however, it is clear that beyond changing the stability the phase, strain and alloying can influence the properties of this family of ferroelectric compounds as well.

4 Conclusions

In this work, we used density functional theory (DFT) calculations to study changes in the stability of a ferroelectric phase in 12 M_2CT_2 MXenes upon chemical substitution of *M* cations and *T* anions. We found that Y_2CO_2, Y_2CS_2 and Sc_2CS_2 are three compounds that having the ferroelectric mixed phase as their ground state, while Sc_2CO_2 displays an asymmetric antiferroelectric phase, leading to agreement between several previous computational studies; we discuss the potential for stabilizing these materials given the results of thermodynamic analyses by previous studies. From calculation of the density of states and Bader charges, we also showed that the out-of-plane polarization in these 2D MXene materials occurs from an orbital overlap between C and the surface atoms. In addition to ferroelectricity, we find that these materials also show good piezoelectric properties; furthermore, the small out-of-plane Born effective charges and the small dielectric constants of the MXenes show agreement with other monolayer 2D materials. Finally, we showed that alloying of the *M* sites and application of external strain can preferentially stabilize the metastable ferroelectric phase. These results lead to a better understanding of these materials and gives agreement between results of different studies in the literature, and will hopefully help in the discovery of new 2D materials with out-of-plane polarizations.

Conflicts of interest

There are no conflicts to declare.

Acknowledgements

Calculations were performed on high performance computing clusters, including: (1) the local cluster, Lochness, at the New Jersey Institute of Technology; (2) the CARBON cluster at the Center for Nanoscale Materials (Argonne National Laboratory), supported by DOE-BES DE-AC02-06CH11357) under allocations CNM68109, CNM72794, and CNM75950, and (3) the Extreme Science and Engineering Discovery Environment (XSEDE), which is supported by NSF Grant No. ACI-1548562, under allocations TG-DMR200002 and TG-DMR190094. Funding was provided by startup funds from the Newark College of Engineering at the New Jersey Institute of Technology.

Notes and references

1 Z. Zafar, A. Zafar, W.-H. Wang, M.-Y. Liu, Z.-H. Ni and Y.-M. You, *ACS Applied Materials & Interfaces*, 2018, **10**, 39187–39193.
2 R. Cuppens, P. Larsen and G. Spierings, *Microelectronic Engineering*, 1992, **19**, 245 – 252.
3 R. C. G. Naber, K. Asadi, P. W. M. Blom, D. M. de Leeuw and B. de Boer, *Advanced Materials*, 2010, **22**, 933–945.
4 S. Mathews, R. Ramesh, T. Venkatesan and J. Benedetto, *Science*, 1997, **276**, 238–240.
5 R. C. G. Naber, B. de Boer, P. W. M. Blom and D. M. de Leeuw, *Applied Physics Letters*, 2005, **87**, 203509.
6 R. Chaudhary, K. Patel, R. K. Sinha, S. Kumar and P. K. Tyagi, *Journal of Applied Physics*, 2016, **120**, 013104.
7 L. Qu, Y. Liu, J.-B. Baek and L. Dai, *ACS Nano*, 2010, **4**, 1321–1326.
8 F. Song and X. Hu, *Nat Commun*, 2014, **5**, 4477.
9 S. Yang, Y. Gong, J. Zhang, L. Zhan, L. Ma, Z. Fang, R. Vajtai, X. Wang and P. M. Ajayan, *Advanced Materials*, 2013, **25**, 2452–2456.
10 Y. Sun, S. Gao and Y. Xie, *Chem. Soc. Rev.*, 2014, **43**, 530–546.
11 C. Wu, X. Lu, L. Peng, K. Xu, X. Peng, J. Huang, G. Yu and Y. Xie, *Nat Commun*, 2013, **4**, 2431.
12 J. Junquera and P. Ghosez, *Nature*, 2003, **422**, 506–509.
13 D. Ji, S. Cai, T. R. Paudel, H. Sun, C. Zhang, L. Han, Y. Wei, Y. Zang, M. Gu, Y. Zhang, W. Gao, H. Huyan, W. Guo, D. Wu, Z. Gu, E. Y. Tsymbal, P. Wang, Y. Nie and X. Pan, *Nature*, 2019, **570**, 87–90.
14 P. Gao, Z. Zhang, M. Li, R. Ishikawa, B. Feng, H.-J. Liu, Y.-L. Huang, N. Shibata, X. Ma, S. Chen, J. Zhang, K. Liu, E.-G. Wang, D. Yu, L. Liao, Y.-H. Chu and Y. Ikuhara, *Nature Communications*, 2017, **8**, 15549.
15 X. Huang, Z. Zeng and H. Zhang, *Chem. Soc. Rev.*, 2013, **42**, 1934–1946.
16 M. Chhowalla, Z. Liu and H. Zhang, *Chem. Soc. Rev.*, 2015, **44**, 2584–2586.
17 Y. Li, S. Tongay, Q. Yue, J. Kang, J. Wu and J. Li, *Journal of Applied Physics*, 2013, **114**, 174307.

18 H. H. Huang, X. Fan, D. J. Singh and W. T. Zheng, *Nanoscale*, 2020, **12**, 1247–1268.

19 S. N. Shirodkar and U. V. Waghmare, *Phys. Rev. Lett.*, 2014, **112**, 157601.

20 Y. Lin, T. V. Williams and J. W. Connell, *The Journal of Physical Chemistry Letters*, 2010, **1**, 277–283.

21 G. Han, Z.-G. Chen, J. Drennan and J. Zou, *Small*, 2014, **10**, 2747–2765.

22 J. van Landuyt, G. van Tendeloo and S. Amelinckx, *physica status solidi (a)*, 1975, **30**, 299–314.

23 C. Cui, W.-J. Hu, X. Yan, C. Addiego, W. Gao, Y. Wang, Z. Wang, L. Li, Y. Cheng, P. Li, X. Zhang, H. N. Alshareef, T. Wu, W. Zhu, X. Pan and L.-J. Li, *Nano Letters*, 2018, **18**, 1253–1258.

24 F. Liu, L. You, K. L. Seyler, X. Li, P. Yu, J. Lin, X. Wang, J. Zhou, H. Wang, H. He, S. T. Pantelides, W. Zhou, P. Sharma, X. Xu, P. M. Ajayan, J. Wang and Z. Liu, *Nature Communications*, 2016, **7**, 12357.

25 A. Chandrasekaran, A. Mishra and A. K. Singh, *Nano Letters*, 2017, **17**, 3290–3296.

26 M. Naguib, M. Kurtoglu, V. Presser, J. Lu, J. Niu, M. Heon, L. Hultman, Y. Gogotsi and M. W. Barsoum, *Advanced Materials*, 2011, **23**, 4248–4253.

27 Y. Meng, Y. Zhao, D. Wang, D. Yang, Y. Gao, R. Lian, G. Chen and Y. Wei, *J. Mater. Chem. A*, 2018, **6**, 5782–5788.

28 A. VahidMohammadi, A. Hadjikhani, S. Shahbazmohamadi and M. Beidaghi, *ACS Nano*, 2017, **11**, 11135–11144.

29 M. H. Tran, T. Schäfer, A. Shahraei, M. Dürrschnabel, L. Molina-Luna, U. I. Kramm and C. S. Birkel, *ACS Applied Energy Materials*, 2018, **1**, 3908–3914.

30 X. Zhan, C. Si, J. Zhou and Z. Sun, *Nanoscale Horizons*, 2020, **5**, 235–258.

31 Y. Cheng, Y. Zhang, Y. Li, J. Dai and Y. Song, *J. Mater. Chem. A*, 2019, **7**, 9324–9334.

32 Z. Guo, J. Zhou, L. Zhu and Z. Sun, *J. Mater. Chem. A*, 2016, **4**, 11446–11452.

33 X. Liang, A. Garsuch and L. F. Nazar, *Angewandte Chemie International Edition*, 2015, **54**, 3907–3911.

34 X. Liang, Y. Rangom, C. Y. Kwok, Q. Pang and L. F. Nazar, *Advanced Materials*, 2017, **29**, 1603040.

35 J. Yan, C. E. Ren, K. Maleski, C. B. Hatter, B. Anasori, P. Urbankowski, A. Sarycheva and Y. Gogotsi, *Advanced Functional Materials*, 2017, **27**, 1701264.

36 V. Armin, R. Johanna and G. Yury, *Science*, 2021, **372**, eabf1581.

37 X. Tang, X. Guo, W. Wu and G. Wang, *Advanced Energy Materials*, 2018, **8**, 1801897.

38 B. Anasori and Y. Lukatskaya, Maria R.and Gogotsi, *Nat Rev Mater*, 2017, **2**, 16098.

39 K. Hantanasirisakul and Y. Gogotsi, *Advanced Materials*, 2018, **30**, 1804779.

40 S. Ma, D. Yuan, Z. Jiao, T. Wang and X. Dai, *The Journal of Physical Chemistry C*, 2017, **121**, 24077–24084.

41 D. Yang, X. Fan, D. Zhao, Y. An, Y. Hu and Z. Luo, *Physica E: Low-dimensional Systems and Nanostructures*, 2019, **111**, 84–90.

42 Y. Zhao, J.-J. Zhang, S. Yuan and Z. Chen, *Advanced Functional Materials*, 2019, **29**, 1901420.

43 C. Lei, X. Xu, T. Zhang, B. Huang, Y. Dai and Y. Ma, *The Journal of Physical Chemistry C*, 2021, **125**, 2802–2809.

44 L. Zhang, C. Tang, C. Zhang and A. Du, *Nanoscale*, 2020, **12**, 21291–21298.

45 D. Wijethunge, L. Zhang and A. Du, *J. Mater. Chem. C*, 2021, –.

46 Z. Wang, N. Ding, C. Gui, S.-S. Wang, M. An and S. Dong, *Phys. Rev. Materials*, 2021, **5**, 074408.

47 P. Hohenberg and W. Kohn, *Phys. Rev.*, 1964, **136**, B864–B871.

48 G. Kresse and J. Furthmüller, *Phys. Rev. B*, 1996, **54**, 11169–11186.

49 P. E. Blöchl, *Phys. Rev. B*, 1994, **50**, 17953–17979.

50 J. P. Perdew, K. Burke and M. Ernzerhof, *Phys. Rev. Lett.*, 1996, **77**, 3865–3868.

51 J. Heyd, G. E. Scuseria and M. Ernzerhof, *The Journal of Chemical Physics*, 2003, **118**, 8207–8215.

52 A. V. Krukau, O. A. Vydrov, A. F. Izmaylov and G. E. Scuseria, *The Journal of Chemical Physics*, 2006, **125**, 224106.

53 A. Togo and I. Tanaka, *Scr. Mater.*, 2015, **108**, 1–5.

54 R. D. King-Smith and D. Vanderbilt, *Phys. Rev. B*, 1993, **47**, 1651–1654.

55 W. Tang, E. Sanville and G. Henkelman, *Journal of Physics: Condensed Matter*, 2009, **21**, 084204.

56 E. Sanville, S. D. Kenny, R. Smith and G. Henkelman, *Journal of Computational Chemistry*, 2007, **28**, 899–908.

57 G. Henkelman, A. Arnaldsson and H. Jónsson, *Computational Materials Science*, 2006, **36**, 354–360.

58 V. Kamysbayev, A. S. Filatov, H. Hu, X. Rui, F. Lagunas, D. Wang, R. F. Klie and D. V. Talapin, *Science*, 2020, **369**, 979–983.

59 A. N. Enyashin and A. L. Ivanovskii, *The Journal of Physical Chemistry C*, 2013, **117**, 13637–13643.

60 Q. Tang, Z. Zhou and P. Shen, *Journal of the American Chemical Society*, 2012, **134**, 16909–16916.

61 R. Resta and D. Vanderbilt, *Theory of Polarization: A Modern Approach. In: Physics of Ferroelectrics. Topics in Applied Physics*, Springer, Berlin, Heidelberg, 2007, vol. 105.

62 J. Young and T. L. Reinecke, *Phys. Chem. Chem. Phys.*, 2017, **19**, 31874–31882.

63 Y. Liu, H. Xiao and W. A. Goddard, *Journal of the American Chemical Society*, 2016, **138**, 15853–15856.

64 Y. Xie, M. Naguib, V. N. Mochalin, M. W. Barsoum, Y. Gogotsi, X. Yu, K.-W. Nam, X.-Q. Yang, A. I. Kolesnikov and P. R. C. Kent, *Journal of the American Chemical Society*, 2014, **136**, 6385–6394.

65 H. Chen, A. D. Handoko, J. Xiao, X. Feng, Y. Fan, T. Wang, D. Legut, Z. W. Seh and Q. Zhang, *ACS Applied Materials & Interfaces*, 2019, **11**, 36571–36579.

66 M. Khazaei, M. Arai, T. Sasaki, C.-Y. Chung, N. S. Venkatara-

manan, M. Estili, Y. Sakka and Y. Kawazoe, *Advanced Functional Materials*, 2013, **23**, 2185–2192.

67 K. Xiong, P. Wang, G. Yang, Z. Liu, H. Zhang, S. Jin and X. Xu, *Scientific Reports*, 2017, **7**, 15095.

68 M. Ashton, K. Mathew, R. G. Hennig and S. B. Sinnott, *The Journal of Physical Chemistry C*, 2016, **120**, 3550–3556.

69 J. Yang, A. Wang, S. Zhang, H. Wu and L. Chen, *Computational Materials Science*, 2018, **153**, 303–308.

70 V. Kamysbayev, A. S. Filatov, H. Hu, X. Rui, F. Lagunas, D. Wang, R. F. Klie and D. V. Talapin, *Science*, 2020, **369**, 979–983.

71 T. Inoshita, S. Jeong, N. Hamada and H. Hosono, *Phys. Rev. X*, 2014, **4**, 031023.

72 U. Yorulmaz, A. Özden, N. K. Perkgöz, F. Ay and C. Sevik, *Nanotechnology*, 2016, **27**, 335702.

73 H. T. Stokes, D. M. Hatch, B. J. Campbell and D. E. Tanner, *Journal of Applied Crystallography*, 2006, **39**, 607–614.

74 A. Roy, R. Prasad, S. Auluck and A. Garg, *Journal of Physics: Condensed Matter*, 2010, **22**, 165902.

75 M. Soleimani and M. Pourfath, *Nanoscale*, 2020, **12**, 22688–22697.

76 D. Wu, A. J. Pak, Y. Liu, Y. Zhou, X. Wu, Y. Zhu, M. Lin, Y. Han, Y. Ren, H. Peng, Y.-H. Tsai, G. S. Hwang and K. Lai, *Nano Letters*, 2015, **15**, 8136–8140.

77 K. F. Garrity, K. M. Rabe and D. Vanderbilt, *Phys. Rev. Lett.*, 2014, **112**, 127601.

78 S. M. Oliver, J. Young, S. Krylyuk, T. L. Reinecke, A. V. Davydov and P. M. Vora, *Communications Physics*, 2020, **3**, 10.

79 A. Chaves, J. G. Azadani, H. Alsalman, D. R. da Costa, R. Frisenda, A. J. Chaves, S. H. Song, Y. D. Kim, D. He, J. Zhou, A. Castellanos-Gomez, F. M. Peeters, Z. Liu, C. L. Hinkle, S.-H. Oh, P. D. Ye, S. J. Koester, Y. H. Lee, P. Avouris, X. Wang and T. Low, *npj 2D Materials and Applications*, 2020, **4**, 29.

80 A. K. Singh, P. Kumbhakar, A. Krishnamoorthy, A. Nakano, K. K. Sadasivuni, P. Vashishta, A. K. Roy, V. Kochat and C. S. Tiwary, *iScience*, 2021, **24**, 103532.